Fireworks in the Primate Retina: In Vitro Photodynamics Reveals Diverse LGN-Projecting Ganglion Cell Types

Neurotechnique

Dennis M. Dacey,[1,*] Beth B. Peterson,[1]
Farrel R. Robinson,[1] and Paul D. Gamlin[2]
[1]Department of Biological Structure
University of Washington
Seattle, Washington 98175
[2]Department of Physiological Optics
University of Alabama
Birmingham, Alabama 35294

Summary

Diverse cell types and parallel pathways are characteristic of the vertebrate nervous system, yet it remains a challenge to define the basic components of most neural structures. We describe a process termed retrograde photodynamics that allowed us to rapidly make the link between morphology, physiology, and connectivity for ganglion cells in the macaque retina that project to the lateral geniculate nucleus (LGN). Rhodamine dextran injected into the LGN was transported retrogradely and sequestered within the cytoplasm of ganglion cell bodies. Exposure of the retina to light in vitro liberated the tracer and allowed it to diffuse throughout the dendrites, revealing the cell's complete morphology. Eight previously unknown LGN-projecting cell types were identified. Cells could also be targeted in vitro for intracellular recording and physiological analysis. The photodynamic process was also observed in pyramidal cells in a rat neocortical slice.

Introduction

Relating a neuron's dendritic morphology and axonal connections to its physiological properties is fundamental to a bottom-up functional characterization of any neural system. A variety of classical techniques, including intracellular recording and staining and retrograde and anterograde tracing methods, have been used to attack the problem, but it remains a technical challenge to clearly link anatomy and physiology to a cell type's functional role in a complex network. Growing recognition of the extreme complexity of mammalian neural systems has provided a still greater challenge to achieving this goal. Thus, the neocortex, whose neuronal diversity was generally appreciated 100 years ago, has only recently been tackled in quantitative detail, with current estimates of the number of distinct cell populations in the range of 100 (Born, 2001; Sawatari and Callaway, 2000). Likewise, the vertebrate retina, traditionally considered a relatively simple and accessible part of the visual system, contains a surprisingly diverse array of distinct cell populations estimated to be between 50 and 80 (Dacey, 2000; Masland, 2001a, 2001b; Masland and Raviola, 2000; Vaney, 1990; Wässle and Boycott, 1991). How do we systematically identify and target

these populations for any useful analysis of structure and function? The great majority of neurons have remained, in fact, technically inaccessible to detailed study or in many cases to any study at all. For example, the output neurons of the retina, the ganglion cells, comprise an estimated 20 anatomically and physiologically unique populations giving rise to a similar number of parallel visual pathways. Yet the morphology, light response properties, and underlying circuitry have been intensively investigated for only a few particularly accessible cell types. One recent approach to an overall understanding of retinal ganglion cells has been to combine retrograde tracing to define the brainstem target with physiological methods—extra- or intracellular recording and/or intracellular dye staining—to define cellular morphology and physiology in an in vitro preparation of the retina (e.g., Pu et al., 1994; Rodieck and Watanabe, 1993; Yang and Masland, 1994). By this approach, ganglion cells retrogradely labeled from tracer injections in a particular structure (for example, the superior colliculus or the LGN) can be selectively targeted for anatomical and/or physiological study in vitro. A limitation of this approach is that retrograde labeling provides little information about the morphology of labeled neurons that would facilitate the identification or selection of any particular cell type for systematic study with other methods. Thus, progress with the method is necessarily slow and the ability to access cell types that are functionally important but exist at relatively low densities is extremely difficult.

Here, we describe a technical discovery that overcomes this problem and greatly facilitates making the link between morphology, physiology, and projection pattern for primate retinal ganglion cells. The method stems from a fortuitous observation during experiments using rhodamine-dextrans to retrogradely label macaque monkey ganglion cells from tracer injections in the major central targets of the retina: the superior colliculus, pretectum, and LGN. Our goal was to identify and physiologically characterize the diverse ganglion cell types that contribute to these pathways but whose functional properties and retinal microcircuitry were unknown (e.g., DeMonasterio and Gouras, 1975). As expected, rhodamine dextran, after transport to the retina, was sequestered into organelle-like structures within ganglion cell bodies and proximal dendrites. This particulate labeling alone did not allow unambiguous targeting of specific cell types in vitro for further study. When, however, labeled cells were observed microscopically under epifluorescent illumination, the fluorescing organelles appeared to burst—creating a firework-like display in the cytoplasm—and the liberated fluorophore rapidly diffused throughout the dendritic tree. At the same time, a large increase in fluorescence intensity within the cytoplasm gave rise to a bright and complete intracellular dye stain. Since photostained cells remain anatomically and physiologically viable, we could exploit photostaining to selectively target morphologically distinct cell types in vitro for intracellular recording and analysis of visual receptive field properties. Further, by employing
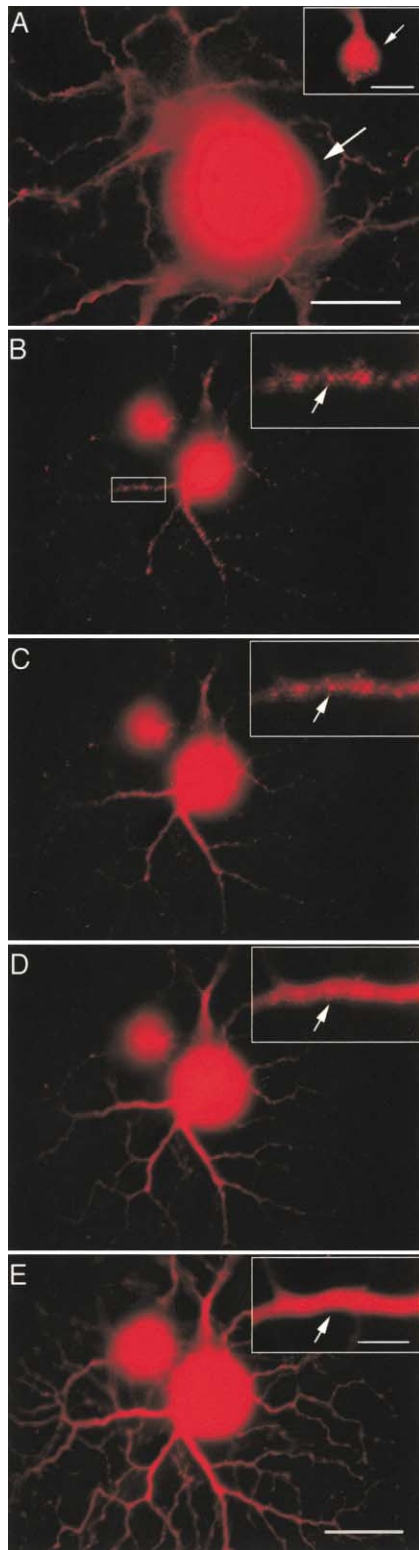
*Correspondence: dmd@u.washington.edu

Figure 1. In Vitro Photostaining of Ganglion Cells Retrogradely Tracer-Labeled Following Injections of Biotinylated Rhodamine Dextran in the Pretectum and the LGN

(A) The pretectum. Photomicrograph in inset was taken just prior to photostaining. Focus is in the ganglion cell layer on the cell body of a previously undescribed cell type. The fluorescent tracer appears as small bright granules restricted to the soma and one proximal

the biotinylated form of rhodamine dextran, it was possible to use horseradish peroxidase (HRP) histochemistry after tissue fixation to permanently recover the detailed morphology and mosaic organization of large numbers of cells for anatomical analysis. This method has made it possible to rapidly characterize a diverse new group of at least eight ganglion cell populations that project in the primary visual pathway to the LGN. Preliminary results in rat cerebral cortex also demonstrate its applicability to the study of neurons in other brain systems. Thus, photodynamic staining of cells retrogradely labeled with biotinylated rhodamine dextran provides a novel in vitro method that permits access to the complex relationship between dendritic morphology, connectivity, and physiological properties for some of the most difficult-to-study neuronal microcircuits.

Results

Retrograde Tracer-Labeling and In Vitro Photodynamic Filling

In the in vitro, intact retina, ganglion cells retrogradely labeled with biotinylated rhodamine-dextran can be easily visualized with epifluorescent illumination. The transported rhodamine initially appears as small fluorescent granules principally in the cell body (Figure 1A inset, arrow), indicating that the tracer is sequestered in an internal compartment, presumably lysosomes (Vercelli et al., 2000). When the cell is briefly exposed ($\sim$1–20 s) to epifluorescent illumination, the distinct granules disappear and the entire dendritic tree becomes intensely and uniformly fluorescent (Figure 1A and see Supplemental Movie at http://www.neuron.org/cgi/content/full/37/1/15/DC1). The process of photodynamic staining can be followed over time with more precision in cells in which tracer granules are also present in the proximal dendrites (Figures 1B–1E). In this case, it is possible to place the plane of focus precisely on the dendritic tree and capture sequential high-resolution images during the photostaining process. Within a few seconds of light exposure, the fluorescent granules grow brighter and appear to suddenly burst (Figures 1B–1E, insets), the intensity of the fluorescence increases greatly, and dye can be observed diffusing throughout the dendritic cytoplasm (Figures 1C–1E). Despite the diffusion of dye within the dendritic tree, a clear and dramatic many-fold *increase* in fluorescence can be observed as the photoreaction proceeds over the course of several seconds. The seemingly paradoxical increase in fluorescence intensity is probably explained

dendrite (arrow). After $\sim$10 s of light exposure, the plane of focus was shifted to the inner plexiform layer (IPL); the finest branches of the cell's dendritic tree appear completely stained and the intensity of the rhodamine fluorescence in the cell body has increased greatly (arrow). Scale bar equals 50 μm in main image and 25 μm in inset. (B–E) The LGN. Plane of focus is on the dendritic tree of a parasol ganglion cell; granules of tracer are present in the proximal dendrites (insets). Photostaining was initiated upon light exposure used to take the photographic sequence and proceeds from (B) through (E): the dendritic granules burst (arrows, insets) and the tracer diffuses rapidly throughout the cytoplasm revealing the entire dendritic tree (E). Scale bar equals 50 μm in the main image and 10 μm in inset.
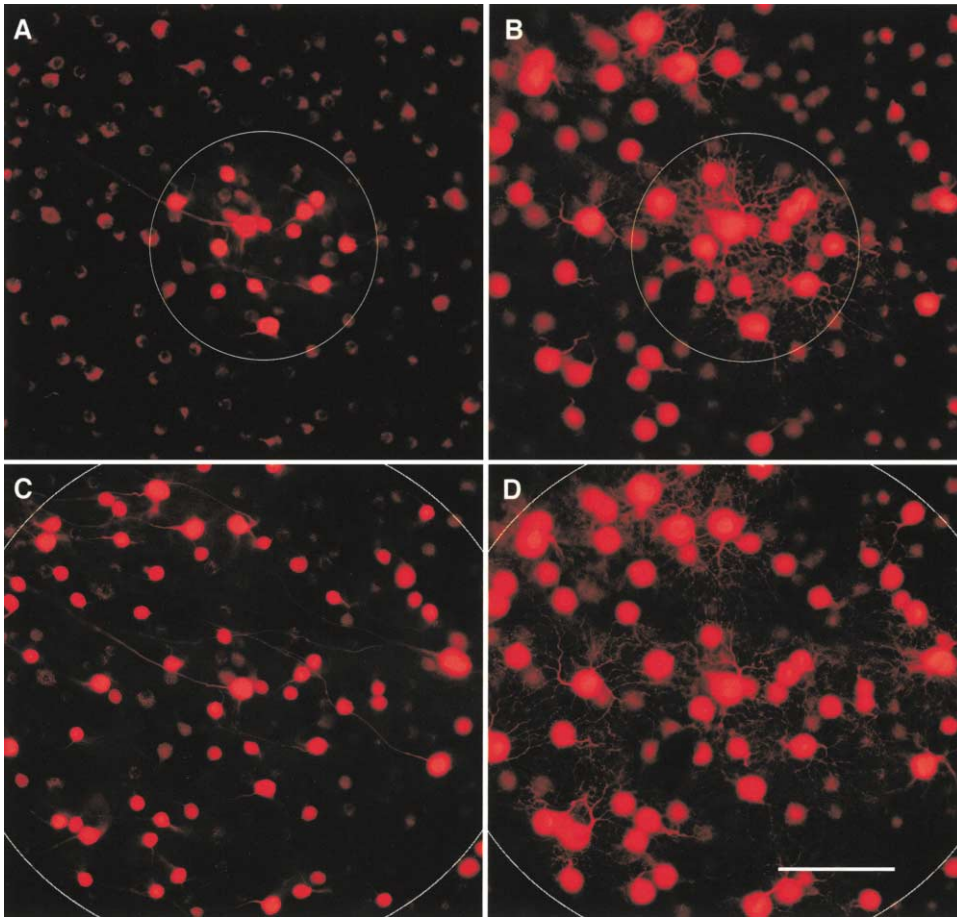
Figure 2. Simultaneous Photodynamic Staining of Clusters of Retrogradely Labeled Cells Can Be Achieved with Low-Magnification Optics

(A) About a 400 × 400 μm field of ganglion cells in vitro that were retrogradely labeled from rhodamine-dextran injections placed in the LGN. The inset circle shows a small field (∼200 μm diameter) illuminated briefly using a 20× objective and with the epilluminator aperture partially closed. Photostaining is initiated and restricted to the labeled cells within the small circular field.

(B) Plane of focus is shifted to the IPL, revealing dendritic arbors of photostained cells. Note that the light exposure (∼1 s) used to take this photograph has initiated photostaining in the larger surrounding field of cells.

(C) Plane of focus is in the ganglion cell layer. Further exposure of the larger field indicated by circle completes the photostaining of this field.

(D) Plane of focus shifted again to the IPL to show dendritic staining. Scale bar equals 100 μm.

by the photochemical process referred to as "self-quenching" and will be considered further in the Discussion.

By varying the amount of retinal surface that is exposed to light, it is possible to photostain single cells, small clusters of cells, or very large patches of retrogradely labeled cells in a controlled way. Groups of labeled neurons can be photostained by exposing larger fields using lower-magnification optics (Figures 2A–2D). There also appears to be some correlation between the rapidity of photostaining and the intensity of retrograde label. Thus, the most intensely labeled neurons photostain completely after a very brief exposure (∼1 s), whereas other more lightly labeled cells may require 10–20 s to initiate photostaining.

The great increase in fluorescence intensity that occurs at the liberation of the fluorophore permits even the finest details of the dendritic structure of photostained cells to be observed in vitro (Figures 3A–3D). Fine dendritic spines, appendages, and branching pat-

terns (Figure 3B), together with subtle changes in depth of dendritic stratification (Figures 3C and 3D), are features that are critical for distinguishing among ganglion cell types. For example, the delicate and subtle dendritic branching pattern, spines, and bistratification that distinguish the color opponent small bistratified cell type (Figures 3C and 3D) from the nonopponent parasol cell type (Figures 3A–3B) are easily appreciated in vitro after photostaining.

Photostaining Reveals Extreme Cell Type Diversity in the Retinogeniculate Pathway
Photostaining of ganglion cells retrogradely labeled from tracer injections made into the LGN revealed a level of complexity not previously appreciated in the retinogeniculate pathway of a primate. Previously unrecognized cell types were identified in vitro by characteristics of dendritic morphology. At least eight morphologically distinct ganglion cell types, in addition to those types that have been recognized classically by other
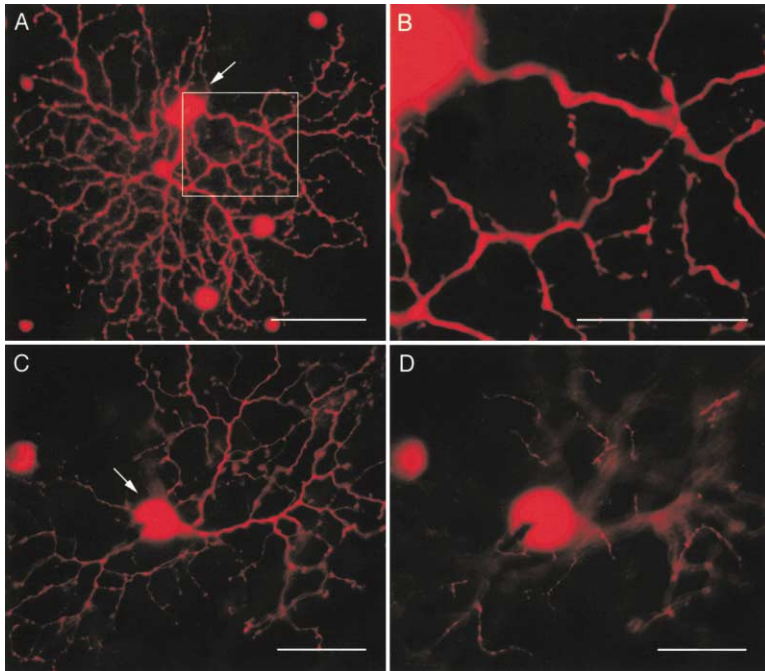
Figure 3. Photodynamic Staining Reveals Fine Dendritic Structure Characteristic of Distinct Cell Types

Cells were retrogradely tracer-labeled following injections of biotinylated rhodamine dextran in the LGN and photographed in vitro.
(A) Photomicrograph of a photostained parasol cell. Inset box is shown at higher magnification in (B).
(B) Photostained dendritic spines and appendages on dendrites of the parasol cell shown in (A).
(C) Photostaining of a small bistratified cell. Focus is on the dendrites in the inner portion of the IPL. This cell is similar in size to the parasol cell in (A) but differs in dendritic detail.
(D) Same cell as shown in (C) but with the focus shifted to where a small number of very fine photostained dendrites can be observed extending to the outer border of the IPL, a characteristic feature of this cell type (Dacey and Lee, 1994). Scale bars in (A), (C), and (D) equal 50 μm. Scale bar in (B) equals 25 μm.

methods (to give a total of 13 ganglion cell populations thus far), could immediately be distinguished in an initial sample of 300+ photostained and HRP-reacted cells and are summarized in Figure 4. Cell population-specific features characterized after photostaining included distinct dendritic branch density and morphology, depth of dendritic stratification in the inner plexiform layer (IPL), systematic variation in dendritic field diameter as a function of retinal eccentricity, and the regular mosaic-like organization of neighboring dendritic trees of like-type (see also Figure 7). Thus, seven ganglion cell types with monostratified dendritic trees and a single type with a bistratified dendritic tree could be distinguished categorically by depth of dendritic stratification; stratification depth covaried with other properties such as dendritic field diameter or branch density to generate an overall picture of the new cell types and to provide the basis for continued anatomical study (Figure 4D) and the addition of any further types. As will be discussed below, initial intracellular recordings from several of these types reveal equally characteristic physiological properties.

Intracellular Recording from Photostained Cells: Morphology Correlates with Physiology

In addition to the preservation of dendritic morphology after photostaining, we found the physiological properties of these cells also to be well maintained. Photostained ganglion cells in our preparation exhibit light responses that are indistinguishable from that of non-photostained cells recorded in vitro. We examined the quality of the intracellular physiology by first recording from photostained parasol ganglion cells. Parasol cells have a distinctive dendritic morphology previously well characterized (e.g., Dacey and Petersen, 1992; Watanabe and Rodieck, 1989) and are easily stained and identified by the photodynamic process after retrograde

labeling from tracer injections in the LGN, a major target of this ganglion cell type (Figures 1B–1E, 3A, and 3B). Parasol cells have been recorded intracellularly and correspond to the physiological M ganglion cell type. The light response properties of this anatomical type are well known (for review, see Lee, 1999). The parasol cell of Figure 5A was recorded intracellularly after photostaining and had a light-adapted resting membrane potential in the normal range (59 mV), a maintained spike discharge characteristic of this ganglion cell type (20–40 spikes/sec), and spatial and temporal properties identical to that recorded either in vitro or in the intact animal (Figures 5B–5D; Dacey and Lee, 1994; Lee et al., 1988, 1990, 1994).

The photodynamic reaction does not appear to alter or degrade physiological activity as significant time passes after photostaining. Cells recorded from long periods maintained a consistent light response; the parasol cell in Figure 5, for example, was recorded intracellularly for ~2 hr and we found no change in the quality of the intracellular physiology.

Beyond the parasol ganglion cells, several other ganglion cell types illustrated in Figure 4 have been recorded, revealing a further correspondence of dendritic morphology with specific physiological properties not previously described for the retinogeniculate pathway. One dramatic example is the large field bistratified ganglion cell type whose dendrites costratify with the small bistratified cell type (Figure 5E). The small bistratified cell has previously been shown to receive excitatory input from S cones and to give a color-opponent blue-ON light type response (Dacey and Lee, 1994). We found that all photostained large field bistratified cells recorded thus far (n = 16) also show a blue-ON type light response and receive excitatory input from S cones, giving an S cone ON, L+M cone OFF opponent response (Figure 5F). The inner stratifying dendritic trees of the

large and small bistratified cells costratify with the axonal arbor of a distinctive cone bipolar cell type that receives selective input from S cones (Figure 4D). By contrast, the large bistratified cell has a correspondingly larger receptive field than the small bistratified cell, consistent with the difference in dendritic field diameter between the two cell types (Figure 4C). The results suggest that the unitary S cone bipolar cell pathway may actually give rise to a family of distinct ganglion cell populations that transmit S cone signals in parallel to primary visual cortex.

Biotin Conjugate Preserves Photodynamic Staining with HRP

In vitro photostaining uniquely permits identification and targeting of morphologically distinct cell types for intracellular recording. By using rhodamine dextran conjugated to biotin, it is also possible to preserve this wealth of morphological detail for subsequent extended analysis after tissue fixation. When biotin is used as part of the tracer, the photostained images created in vitro are translated into a permanent HRP reaction product with no loss of cellular detail (Figure 6). Indeed, the HRP reaction product, as is well known, provides the ideal approach to further characterizing photostained cells anatomically. Following the in vitro experiment, the retina is fixed and processed for the HRP/DAB reaction (see Experimental Procedures). When retrogradely labeled cells are not photostained in vitro, the biotin label remains confined to small dark spots in the soma (Figure 6A), just as the fluorescent label was initially confined to small fluorescent spots in the soma in the in vitro retina (Figure 1). Cells that are photostained in vitro, however, exhibit a dark and evenly distributed HRP staining throughout the soma (Figure 6B) and the dendritic tree is also completely stained (Figures 6C and 6D).

The morphology of biotin-labeled cells recovered following in vitro photostaining has a delicate quality with even the very finest dendritic structures clearly visible (Figures 7A and 7B). The ability to photostain and recover the morphology of large numbers of cells provides an excellent tool for obtaining key features of a cell type that are only discernable when the entire population of cells that comprise the type is revealed (Vaney, 1990). For example, spatial density, cell to cell spacing, and dendro-dendritic interactions are all population features of functional significance. After photostaining, the spatial densities and dendritic overlap of neighboring cells, as well as the arrangement of differently stratifying pairs of cells, can easily be determined (Figure 7C). One of the most useful features of acquiring detailed anatomy in vitro is to generate hypotheses that can be tested by designing appropriate visual stimuli. For example, in one population of retrogradely labeled cells we observed dendritic branching, stratification, and unique patterns of dendritic fasciculation characteristic of ON direction-selective cells previously identified in the rabbit retina (Figure 7D; He and Masland, 1998); it thus becomes of critical importance to use directional stimuli to test the hypothesis that these cells correspond to a primate directionally selective ganglion cell type.

General Applicability of Photodynamic Staining in Other Neuronal Populations

An important question is whether the photostaining that we have described in retrogradely labeled retinal ganglion cells can be applied to other projection neurons in other types of in vitro preparations. We tested this by making biotinylated rhodamine dextran injections into rat primary visual cortex and observing retrograde label in extrastriate cortical pyramidal cells and thalamic relay cells. Preliminary results in rat show that both pyramidal cells (Figure 8) and thalamic relay cells (not shown) were easily observed and photostained in an in vitro brain slice preparation. As for retinal ganglion cells, the fluorescent tracer initially appears as small bright spots in the soma that then appear to burst upon exposure to epifluorescent illumination (Figure 8, inset), and the cell rapidly fills with tracer, revealing its complete dendritic morphology.
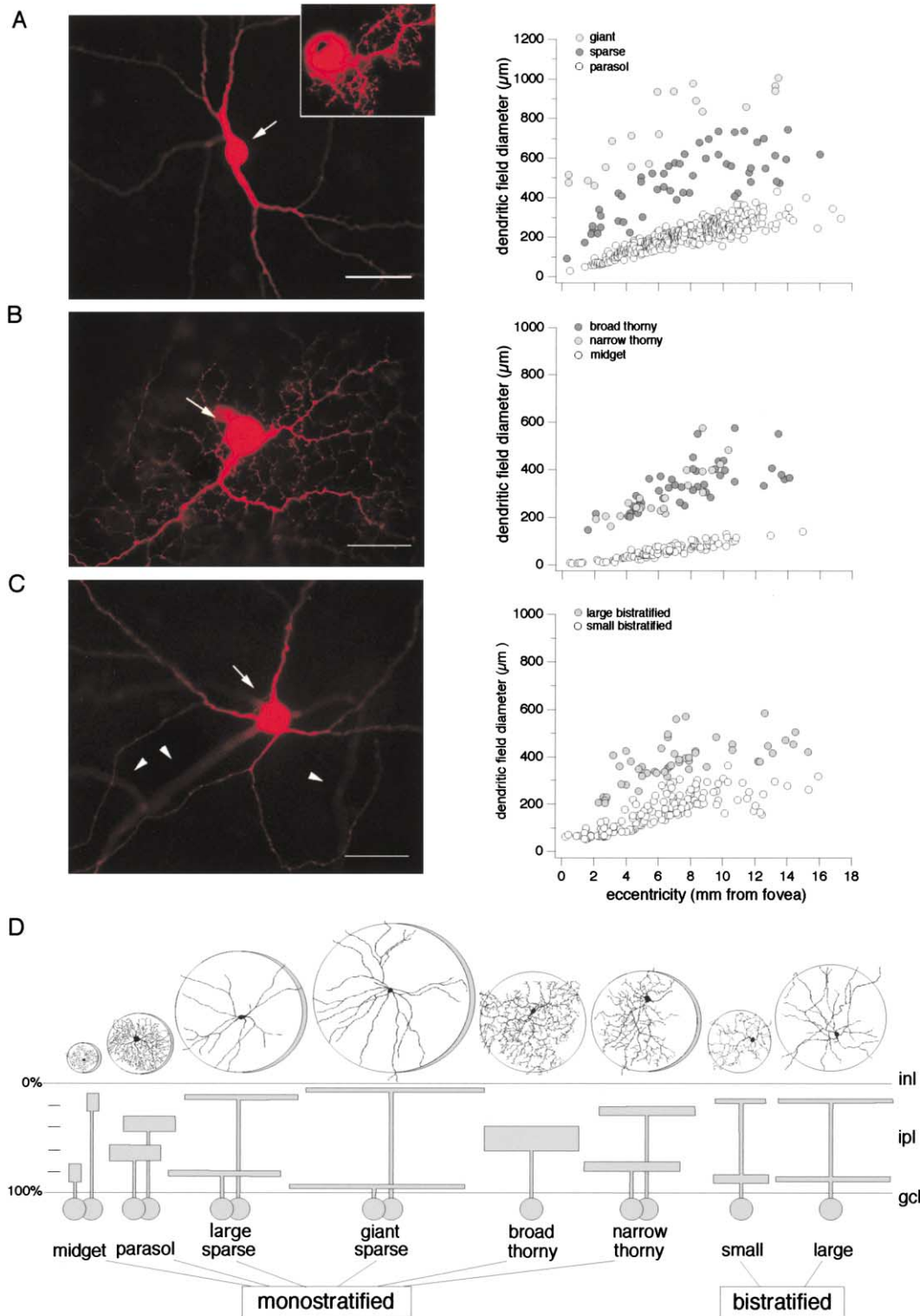
General Remarks

Not all fluorescent dextrans lend themselves to the retrograde labeling and in vitro photostaining described here. We have used both the smaller (3000 mw) and the larger (10,000 mw) biotinylated rhodamine dextrans (see Experimental Procedures) and have found that the smaller molecular weight tracers give a much stronger retrograde label than the larger tracers (Reiner et al., 2000). And while photostaining was a clear property of the rhodamine conjugates, fluorescein-dextrans did not show this property. In two experiments, we injected the pretectum with rhodamine-dextran and the superior colliculus with fluorescein-dextran. In both cases, ganglion cells retrogradely labeled with rhodamine tracers were strongly fluorescent in vitro and easily photostained, but we were never able to stain any cells labeled with fluorescein-dextran. The fluorescein-labeled cells were weakly fluorescent and the fluorescence was quickly quenched upon illumination.

Cell damage from overexposure to epifluorescent illumination is a concern in all tissue preparations that use fluorescent markers. To prevent cell damage from overexposure, in vitro photostaining can easily be monitored through the microscope objective. We have found that strongly labeled cells exposed for a few seconds—just enough illumination to begin photostaining—will often continue filling without further illumination. That is, one can observe the burst of fluorescence in the soma and the beginning of tracer filling in the proximal dendrites, turn the light off, wait ∼10–20 s, then turn the light on and see the entire dendritic tree strongly labeled. In our experience, rhodamine dextran-labeled cells completely photostain using far less illumination than required to produce observable cell damage.

Discussion

The rhodamine-based photodynamic intracellular staining described here has novel advantages for the study of nervous system organization. First, on the purely anatomical side, the detailed morphology of large numbers of neurons can be rapidly acquired and the distinctive morphological features of entire cell populations can be characterized. In the case of the macaque retina, the

Figure 4. Photodynamic Staining Reveals Ganglion Cell Populations Retrogradely Labeled from Tracer Injections Placed in the LGN

At least 13 ganglion cell types can be distinguished by dendritic field size, branching density, and depth of stratification in the IPL.
(A) Photomicrograph at left illustrates the dendritic morphology of a large, sparsely branching monostratified cell; inset shows a photostained midget cell for comparison. The large sparse cells could be divided into four distinct types by depth of stratification in the IPL and dendritic field size (see also D). Scatterplot at right shows dendritic field diameter as a function of retinal eccentricity, comparing field size of giant (light gray symbols; n = 19) and large sparse cells (dark gray symbols; n = 65) to that of parasol cells (open symbols; n = 333).
(B) In vitro photomicrograph of a monostratified "thorny" ganglion cell with a high density of very fine dendritic branches, appendages, and spine-like structures. Thorny cells could be divided into three populations based on branch density and depth of stratification in the IPL.

spatial densities and geometric arrangements of distinct ganglion cell types are needed to build a picture of the synaptic organization and function of retinal microcircuitry (e.g., Sterling, 1998). Second, morphologically identified cells can be targeted for physiological analysis. In most methods when cells are targeted for intracellular recording, with few exceptions, little is known about the morphology or connectivity of the targeted cell. Making the connection between these features is a difficult process that requires luck as well as experimental skill (e.g., Dacey and Lee, 1994; Pu et al., 1994; Yang and Masland, 1994). By contrast, the in vitro photostaining reveals the dendritic morphology of large numbers of cells of a single type, and it is relatively easy to systematically sample these cells with recording electrodes in a way that was not previously possible. Finally, because the photodynamic staining occurs after retrograde transport, an immediate link between an anatomically and physiologically distinct neural population and its long-range connectivity can also be made. This will prove invaluable for understanding the relationship between diverse retinal microcircuits and the parallel visual pathways they give rise to. For example, we have recently used retrograde photodynamics to determine the anatomical and physiological properties of a distinctive "pupillomotor" ganglion cell population retrogradely labeled from the pretectal olivary nucleus, a structure that is the afferent limb of the pupillary light reflex (Gamlin et al., 2001), and we continue to investigate the color-coding properties of the new LGN-projecting ganglion cell populations described here (Dacey et al., 2002).

Cell Type Diversity in the Retinogeniculate Pathway Revealed by Retrograde Photodynamics

The picture of the macaque primary visual pathway revealed here diverges sharply from the classical view, though our results are not unanticipated. It is well established in primate that the retinogeniculate pathway links the two midget ganglion cell populations to the parvocellular LGN layers and the two parasol cell populations to the magnocellular LGN subdivision (for review, see Kaplan et al., 1990). However, morphological evidence for additional LGN-projecting ganglion cell types (Rodieck and Watanabe, 1993), together with the more recent identification of the population of small bistratified, color-opponent ganglion cells (Dacey and Lee, 1994) that likely project via the koniocellular LGN (Martin et al., 1997; White et al., 1998), suggested strongly that the total number of ganglion cell types that contribute to the retinogeniculate pathway was not completely understood. The overall complexity of the macaque ganglion

cell types revealed here is also entirely consistent with the growing understanding of the overall diversity of ganglion cell populations in other mammals. Thus, the emerging picture of the total number of ganglion cell types in the mammalian retina is on the order of 15–20 (Masland, 2001a; Sterling, 1998; Rodieck, 1998). Our observation of at least 13 distinct retinogeniculate ganglion cell populations suggests that the geniculate receives input not from a small number of ganglion cell types but from the majority, if not all, ganglion cell types. A now achievable goal will be to complete the picture of the primate visual pathway by using retrograde photodynamics to characterize the remaining cell populations that project to other brainstem targets of the retina, including the pretectum and superior colliculus, and the degree to which macaque ganglion cells project to multiple targets via collaterals, along with the critical physiological properties of each type.

Recognition of the complexity of the retinogeniculate pathway highlights the strength of the retrograde photodynamic method. Previous experiments using traditional methods of retrograde transport did not provide the number of cells or morphological detail required to identify these types (e.g., Perry et al., 1984); more recent use of intracellular staining in vitro provided the needed morphology, but the number of cells sampled was too low to reveal a complete picture of this pathway (e.g., Rodieck and Watanabe, 1993).

Mechanism of Photodynamic Staining: A Noncytotoxic Dye-Sensitized Photoreaction

The molecular basis for photodynamic liberation and consequent neuronal staining by the rhodamine fluorophore is not known, but a simple, parsimonious hypothesis derives from photochemistry basics (Wayne and Wayne, 2001). Rhodamine, a xanthene dye, is a photosensitizer that, when excited by appropriate wavelengths, can transfer excitation energy to other molecules, producing reactive chemical species including singlet oxygen, a highly reactive and cytotoxic form of molecular oxygen that can cause cell damage and cell death (Diwu and Lown, 1994). Indeed, the properties of a large variety of photosensitizing agents, including various forms of rhodamine, have been exploited in photodynamic therapy (PDT)—a clinical method used to selectively kill tumor cells (Ackroyd et al., 2001). In PDT, a photosensitizer such as rhodamine 123—a specific stain for mitochondria—is accumulated by tumor cells with some selectivity. Subsequent light delivery to the tissue is then used to generate a cytotoxic effect.

We hypothesize that the cell-killing photoreactions exploited in PDT are similar to what we directly observe

---

Broad thorny cells were broadly stratified across the middle of the IPL; narrow thorny cells were more narrowly stratified in the inner and outer portions of the IPL (see also D). Scatterplot at right compares field size for broad thorny (dark gray symbols; n = 39) and narrow thorny (light gray symbols; n = 26) cells with midget ganglion cells (open symbols; n = 93).
(C) Ganglion cell with a large, sparsely branching, bistratified dendritic tree; plane of focus is on inner stratifying dendrites (see also D); outer stratifying dendrites are out of focal plane (arrowheads). Scatterplot at right compares dendritic field size of previously described small bistratified cell (open symbols; n = 163) with the large bistratified cell (closed symbols; n = 53). Soma indicated by arrow in (A)–(C); scale bars equal 50 μm.
(D) Schematic summary of depth of dendritic stratification and mean dendritic field size for each of the 13 ganglion cell populations recognized thus far.
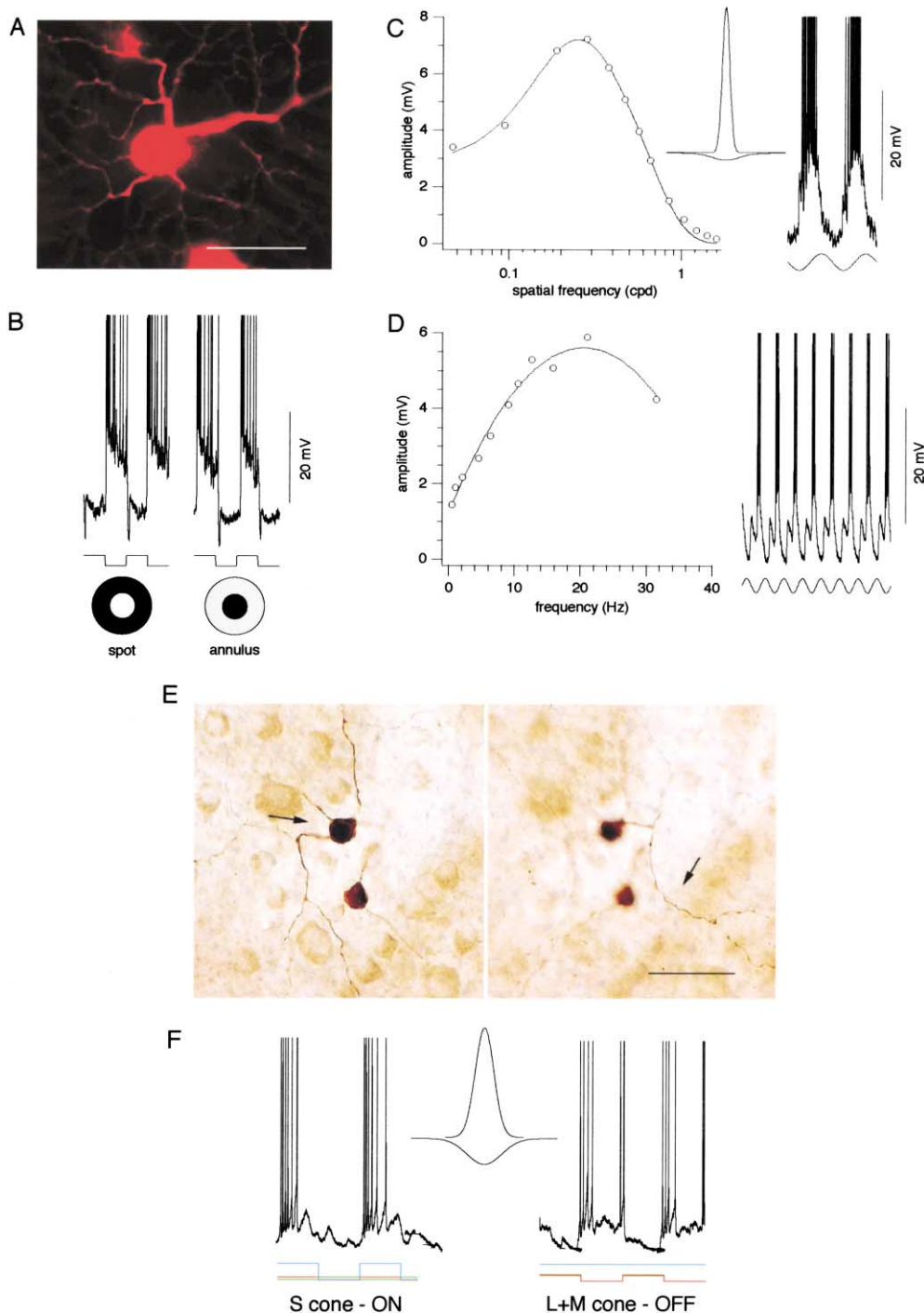
Figure 5. Photostained Ganglion Cells Show Characteristic Light Responses when Recorded In Vitro

(A)–(D) illustrate aspects of the spatial and temporal response properties of an OFF-center parasol ganglion cell photostained prior to intracellular penetration and voltage recording.

(A) In vitro photomicrograph of recorded cell taken after recording was complete and electrode was withdrawn from cell. Dendritic field diameter equals 240 μm. Scale bar equals 50 μm.

(B) Intracellular recording in response to a spot or annulus centered on receptive field shows OFF-center (left trace), ON-surround (right trace) light response; square wave below voltage trace shows time course of 2 Hz modulated stimulus; icons situated below trace illustrate spatial configuration of stimulus.

(C) Sinusoidally modulated gratings varied in spatial frequency and drifted across the receptive field at 2 Hz temporal frequency were used to obtain a spatial frequency response (left, open circles; spatial frequency given as cycles per degree). Solid line is the difference of Gaussians model fit to the data and used to construct a one-dimensional plot of the center and surround receptive field profiles (middle inset) (see Experimental Procedures). The model gives a Gaussian receptive field diameter of 204 μm. Voltage trace (right) shows response to two
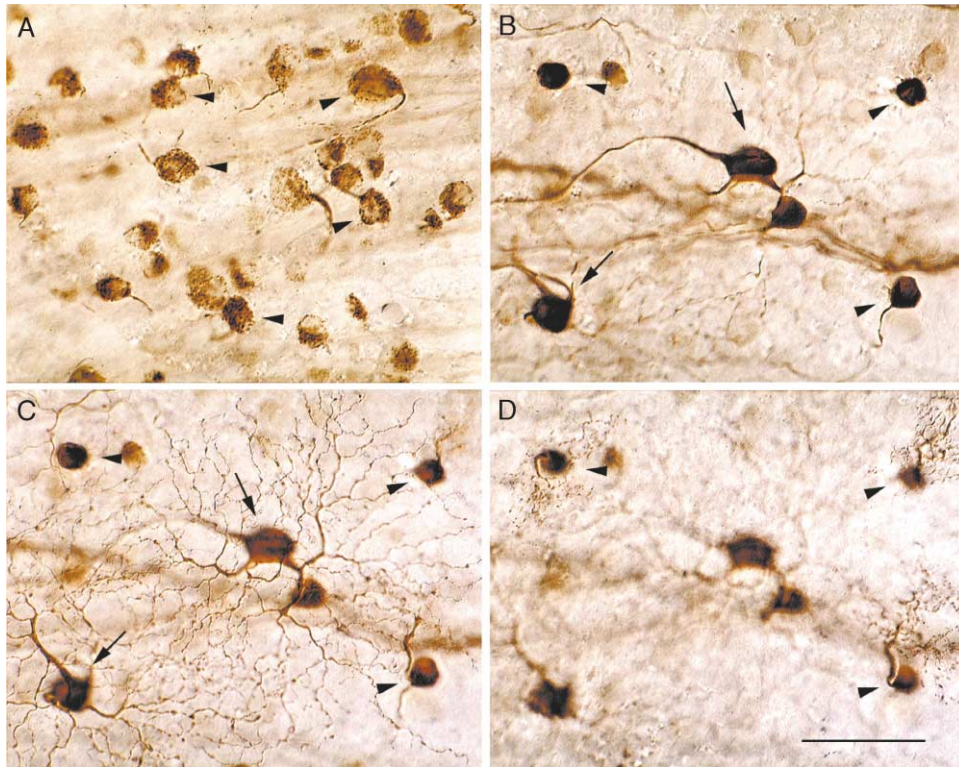
Figure 6. Application of HRP Histochemistry to Photostained Ganglion Cells

When biotin-conjugated rhodamine dextran is used as a tracer, HRP histochemistry can be used to localize and preserve retrograde label after tissue fixation.

(A) Focus is on biotin-labeled cells in the ganglion cell layer. These cells were not photostained in vitro. The biotin label is confined to small brown aggregations in the soma (arrows), just as the fluorescent label was confined to small bright spots in the soma in the in vitro retina (see Figure 1).

(B) Biotin-labeled cell bodies in the ganglion cell layer at a different location in the same retina. These cells were photostained in vitro. Somas are much darker and more evenly labeled than the nonphotostained cells in (A). Arrows indicate somas of two darkly stained parasol cells; arrowheads indicate somas of three midget cells.

(C) Same cells as in (B) but with the focus shifted to the inner portion of the IPL. Photostaining has completely labeled the dendritic trees of the two parasol cells (arrows).

(D) Focus is shifted to the outer portion of the IPL. The dendritic trees of the three midget cells are also completely labeled. Scale bar equals 50 μm.

in the cytoplasm of ganglion cells that have been retrogradely labeled with rhodamine. The rhodamine dextran conjugate is sequestered in an internal compartment in the cell body. We propose that photoexcitation of the fluorophore leads to the creation of reactive oxygen species which in turn damage the cellular structure that is locally concentrating the fluorophore—thus, the striking firework-like display that leads to the liberation and diffusion of the fluorophore within the cytoplasm. The photodynamic effect in vitro is distinct from PDT in that the cellular changes are not obviously cytotoxic; photostained ganglion cells continue to display normal morphology and show the expected light responsiveness and receptive field properties when recorded intracellularly. This benign effect of the photoreaction may be due to tetramethylrhodamine, the form of rhodamine used in the dextran conjugate, being an inherently weaker photosensitizer than the dyes used in PDT (Gan-

---

stimulus cycles at peak sensitivity. Stimulus time course is shown beneath voltage trace.

(D) Temporal frequency response of synaptic potential (open circles) is shown in plot on the left (solid line is a polynomial fit to the data); full field (2 × 3 mm on retinal surface) sine wave modulated stimuli were used. Voltage trace on the right shows the peak response at 21 Hz. Stimulus time course is shown beneath voltage trace.

(E) and (F) illustrate the morphology and light response of a large field bistratified cell like those shown in Figure 4C.

(E) Photomicrograph of a darkly stained cell that was retrogradely labeled from tracer injections placed in the LGN and then processed for standard HRP histochemistry. The soma (arrow) and inner dendrites are shown on the left; the outer dendrites (arrow) are shown on the right. Dendritic field diameter equals 415 μm. Scale bar equals 50 μm.

(F) The cell gave an ON response to 1 Hz square wave chromatic stimuli modulated to isolate S cones (left trace) and an OFF response to stimuli modulated to isolate L+M cones (right trace). A difference of Gaussians model fit to spatial frequency response data (not shown) was used to construct the one-dimensional center and surround receptive field profiles shown in the middle inset. The model gives a Gaussian receptive field diameter of 510 μm.
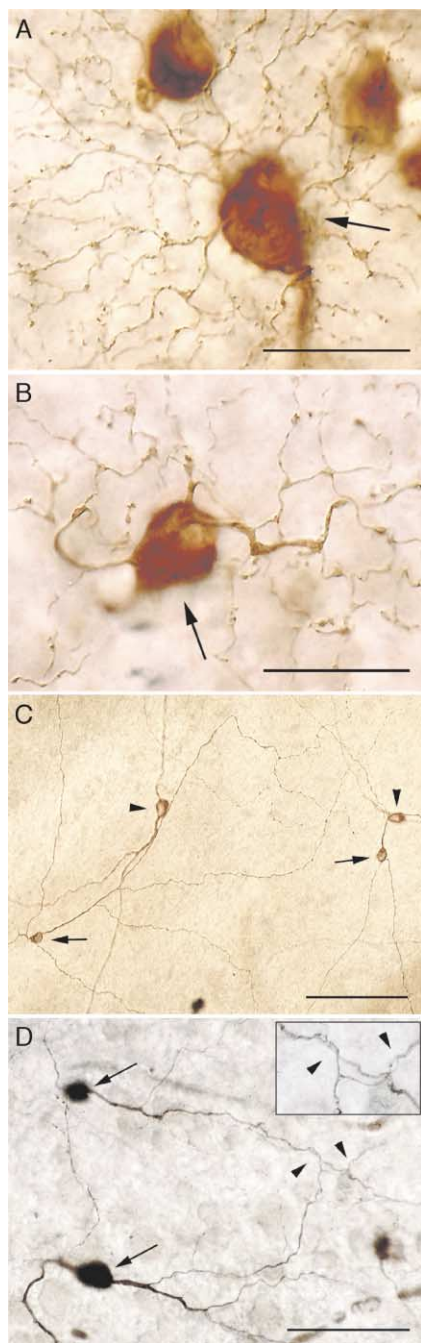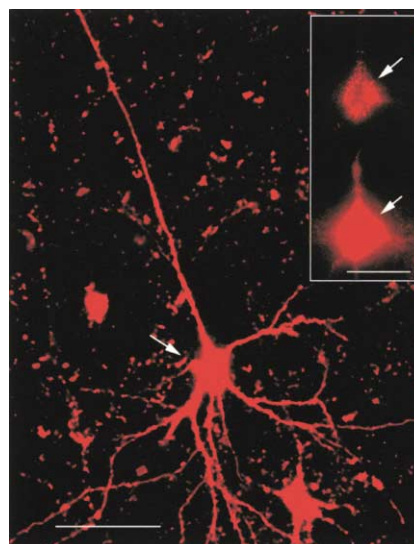
Figure 8. Photodynamic Staining Can Be Successfully Applied to In Vitro Preparations of Other Brain Structures

In vitro photomicrograph of a photostained cortical pyramidal cell (arrow) in a rat brain slice preparation. The cell was retrogradely tracer labeled following injections of biotinylated rhodamine dextran in rat primary visual cortex. Photostaining reveals the entire dendritic arbor of this cell, located in layer 2/3 of extrastriate cortex. Scale bar equals 40 μm. The inset shows another pyramidal cell just prior to (arrow, top photomicrograph) and shortly following (arrow, lower photomicrograph) photostaining. Scale bar equals 25 μm.

din et al., 1983; Diwu and Lown, 1994). Also, the organelle in which rhodamine dextran is sequestered is probably the lysosome (Dougherty et al., 1998; Vercelli et al., 2000), which is thought to be a less cytotoxic site for photosensitizer activity than the subcellular sites usually targeted in PDT—typically mitochondria or the plasma membrane.

The apparent paradoxical increase in fluorescence throughout the cell as the fluorophore diffuses down a concentration gradient can also be explained by the known chemistry of fluorescent systems. In dilute solutions, fluorescence is proportional to dye molecule concentration, but if concentrations reach millimolar levels, "self-quenching" of the fluorescence occurs due to interactions among the fluorophore molecules. Self-quenching is usually a phenomenon to be avoided. However, the reverse effect—the great increase in fluorescence after intracellular release of a trapped fluorescent probe sequestered at high concentrations—has been experimentally demonstrated in neurons of the frog retina (Weinstein et al., 1977). Similarly, in macaque retina,

Figure 7. Photostaining and Subsequent HRP Histochemistry Preserves Fine Details of Dendritic Structure and Reveals Mosaic Organization of Identified Cell Populations

(A and B) High-magnification photomicrographs showing dendritic details of two ganglion cells retrogradely tracer-labeled with biotinylated rhodamine dextran from injections in the LGN, photostained in vitro, and processed for the HRP reaction. Scale bars equal 25 μm.
(A) Soma (arrow) and dendrites of an inner parasol cell.
(B) Soma (arrow) and inner dendritic arbor of a small bistratified cell.
(C) Lower-magnification photomicrograph of previously undescribed ganglion cell types retrogradely labeled from tracer injections placed in the pretectum. Focus is on the dendrites and somas of two neighboring large, sparsely branching, outer stratifying cells with somas displaced to the IPL (arrows). The out-of-focus somas and dendrites of two neighboring large, sparsely branching, inner

stratifying cells are indicated by arrowheads. Scale bar equals 100 μm.
(D) Previously undescribed wide-field cells (arrows) with moderately branched, inner stratifying dendritic trees retrogradely labeled from tracer injections placed in the LGN. The inset shows an area of overlapping dendrites at higher magnification where the dendrites of these neighboring cells appear to fasciculate (arrowheads), a characteristic not seen in the cells illustrated in (A)–(C) but a feature commonly described for direction selective ganglion cells (see Discussion). Scale bar equals 50 μm.

when the retrogradely transported rhodamine is photo-liberated by destruction of the sequestering organelle, the fluorescence intensity appears to increase by at least an order of magnitude—thus, the fireworks and complete intracellular stain that results.

Because of cytoxicity, previous applications of dye-sensitized photoreactions in the nervous system have focused mainly on targeted cell ablations by intracellular dye injection (for review, see Spikes, 1991; Miller and Selverston, 1979), extracellular application (Picaud et al., 1990, 1993), or the more recent use of targeted gene transfer to get the dye into a neural population before light exposure (Nirenberg and Cepko, 1993; Nirenberg and Meister, 1997). These methods all take advantage of the phototoxic effects of the fluorophores used. Photooxidation reactions have been used to gain information about the morphology of neurons in two situations. Neurons filled with a fluorescent probe have been used to photooxidize diaminobenzidine to create a reaction product that stains the neurons after tissue fixation (Sandell and Masland, 1988). And, in a novel application to study the morphology of rabbit retinal amacrine cells (MacNeil and Masland, 1998), a photooxidation reaction was used to locally convert the nonfluorescent H_2Rhodamine123 to the fluorescent Rhodamine123; when the photoconversion was generated in the light-exposed cell body, the Rhodamine123 diffused throughout the cytoplasm to reveal dendritic morphology. While these methods are extremely useful, they are currently limited to an anatomical picture of the cells studied.

Conclusion

In vitro photodynamic staining of retrogradely transported rhodamine conjugates falls into the broad category of dye-sensitized photoreactions that have been applied to the nervous system. In the great majority of these methods, the goal is to exploit the cellular toxicity of photosensitized reactions as a method of selectively ablating neurons or neural tissue. By contrast, here we have shown how a dramatic photodynamic effect observed in vitro can be used in physiologically viable neurons to make links between a neuron's morphology, physiology, and connectivity not achievable with other current methods.

We have exploited photodynamic staining in the in vitro monkey retina to extend our understanding of the ganglion cell population. We have also been able to show that photodynamic staining can be successfully applied to brain slice preparations in rat, demonstrating that it should be possible to achieve photodynamic staining in any invertebrate or vertebrate neural system that can be maintained in vitro, where identified connections need to be targeted for anatomical and physiological analysis (e.g., Briggs and Callaway, 2001). Since the mechanism for photodynamic staining resides in the fundamental processes of photochemistry, it is likely that, in addition to rhodamine-dextran, other retrogradely transportable photosensitizers with novel properties await discovery (Diwu and Lown, 1994).

Experimental Procedures

Central Injections
Experiments were performed on 20 adult macaque monkeys. Targeted sites were the LGN (10 animals), the pretectum (6 animals),

the superior colliculus (2 animals), and the pretectum and superior colliculus (2 animals). For experiments on alert, behaving monkeys (10 animals), the animal was anesthetized and a stainless steel chronic recording chamber was implanted over a hole in the skull during aseptic surgery. Using a stereotaxic device, the chamber was directed at an angle appropriate for the targeted site and secured to the skull. Following implantation, the animal was mildly sedated with Ketamine and injection sites were identified by recording extracellular potentials in response to light stimuli while advancing an electrode through the recording chamber. Tracer injections were made through the same guide tubes used for recording, using either a 1 μl Hamilton syringe with a 26-gauge needle attached or a length of 32-gauge hypodermic tubing with a pulled-glass micropipette tip (ID ~25 μm) glued over one end.

For experiments on anesthetized animals during acute surgery, animals were anesthetized with isoflurane (1.0%–2.0%) and prepared for recording in an aseptic surgery by positioning the head in a stereotaxic device. A small craniotomy was made over the LGN on both sides. Eyelids were held open with a suture to the skin of the brow and corneas kept moist with applications of ophthalmic ointment. A stereotaxic arm was used to set the anterior-posterior and medial-lateral position of the electrode or pipette. The position of the LGN was determined by recording responses to flashes of light using either an epoxy-coated etched tungsten electrode or a modified injection pipette. The latter was an 80 mm length of 26-gauge stainless steel tubing beveled at the tip to 30° and coated with epoxy. A small region on the beveled tip was exposed to enable recording (pipette impedance = 10–50 kΩ at 1 KHz). Multiple tracks were injected in each LGN. Following injections, the skull was closed with gel foam and the skin sutured and/or wound clips applied.

Injection solutions were 10% biotinylated dextran-conjugated tetramethylrhodamine 3000 mw (micro ruby, #D-7162; Molecular Probes, Eugene, OR) in distilled water or sterile saline. For double labeling, the pretectum was injected with 5% 10,000 MW biotinylated dextran-conjugated tetramethylrhodamine (mini ruby #D-3312; Molecular Probes) and the superior colliculus with 5% biotinylated dextran-conjugated fluorescein 10,000 MW (mini emerald #D-7178; Molecular Probes). A total volume of 0.5–1.0 μl of tracer was used for each injection. Target areas usually received more than one injection, with the injections spaced 0.5–1 mm apart.

Following a survival time of 4 to 7 days, the animal was deeply anesthetized with barbiturate and the eyes removed for in vitro experiment as described below. The animal was perfused through the heart with 800 ml of warm (~37°C) normal saline followed immediately by 4 l of cold (~4°C) 4% paraformaldehyde. The animal was then perfused with 1 l each of 10%, 20%, and 30% sucrose solutions. Frozen sections of the brain were cut and reacted to reveal biotin labeling as described below for retina processing.

One experiment was performed in rat cerebral cortex. Experimental procedures were approved by the University of Alabama at Birmingham IACUC and complied with the USPHS Policy on Humane Care and Use of Laboratory Animals. Two 3-month-old Sprague-Dawley rats were deeply anesthetized and 0.8 μl injections of 10% biotinylated dextran-conjugated tetramethylrhodamine 3,000 MW were made in three sites in primary visual cortex in each. After a 1 week survival time, the animals were euthanized, the brains removed, and vibratome sections were made at a thickness of 250 μm in one animal and 400 μm in the other (Chattipakorn and McMahon, 2002).

In Vitro Photostaining and Recording
The in vitro whole-mount retina preparation has been described previously (Dacey and Lee, 1994; Dacey et al., 1996). In brief, eyes were removed from deeply anesthetized animals prior to saline perfusion. The retina was dissected free of the vitreous and sclera in oxygenated Ames' Medium (Sigma Chemical Co., St. Louis, MO), and the retina-RPE-choroid was placed flat, vitreal surface up, in a superfusion chamber mounted on the stage of a light microscope. Rhodamine-labeled cells were visualized with a green filter block (excitation filter 545 nm; barrier filter 590 nm); fluorescein-labeled cells were visualized with a blue filter block (excitation 490 nm; barrier 515 nm).

Initially, the fluorescence label in vitro was confined to small bright

spots in the soma and proximal dendrites. Labeled cells were photo-stained by brief exposure ($\sim$10–40 s) to epifluorescent illumination ($\sim$7.5 $\times$ 10^{13} photons/μm^2/sec measured at the retinal surface using a CVI spectrophotometer, 20$\times$ objective, 100W mercury vapor lamp, and green filter block) during which the spots appeared to burst; the fluorescence became brighter and uniform in appearance and rapidly diffused throughout the entire cell. Using a 20$\times$ or 40$\times$ objective, groups of neighboring cells were photostained simultaneously while monitoring the photostaining process through the microscope lens to prevent cell damage from overexposure. Usually only a brief exposure was needed to start the photostaining process, which then continued without further illumination until the entire cell was filled. A CCD camera attached to the camera port of the microscope was used to take in vitro images of the photostaining process.

The rat cortical slice preparation has been described elsewhere (Chattipakorn and McMahon, 2002). Briefly, slices were placed in a superperfusion chamber mounted on the stage of a light microscope and maintained in standard artificial CSF saturated with 95% O$_2$ and 5% CO$_2$ (pH 7.4), 28°C–30°C, and with a constant perfusion rate of 2–3 ml/min. Rhodamine-labeled cells were observed and photostained in the same manner as described above for macaque retinal ganglion cells.

Labeled cells were targeted for intracellular recording using microelectrodes filled with a solution of 2%–3% Neurobiotin (Vector Labs, Burlingame, CA) and 1%–2% pyranine (Molecular Probes) in 1.0 M potassium acetate. Electrical impedances ranged from 300–450 MΩ. Square and sine wave stimuli with precisely known temporal and chromatic properties were created using a digital light projector. The stimuli were relayed by an optical system to the camera port of the microscope and imaged on the retina by a microscope objective. The visual stimulator is described in detail elsewhere (Packer et al., 2001).

Sinusoidal gratings and receptive field modeling used to determine the spatial receptive field properties illustrated in Figures 5C and 5F are described elsewhere (Dacey et al., 2000). In brief, drifting sinusoidally modulated gratings of varying spatial frequency were used. For each spatial type, a series of stimuli was presented, and the cell's response was measured as a function of the spatial parameter. Within a series, the modulation contrast (100%) and temporal frequency (2 Hz) were held fixed. All stimulus modulations were isochromatic (CIE 1931 chromaticity x = 0.304, y = 0.349) around a background with the same chromaticity and a mean luminance of $\sim$1000 td. Response amplitudes to a grating series were used to determine the parameters of a difference of Gaussians receptive field model (Enroth-Cugell et al., 1983).

Histology

Following an experiment, retinas were dissected free of the RPE and choroid, fixed for 2 hr in 4% paraformaldehyde, and rinsed overnight in phosphate buffer (0.1 M, pH 7.4). Retinas were incubated in 0.1% Triton X-100 (pH 7.4) containing the Vector avidin-biotin-HRP complex (Elite kit, Vector Labs) for 8 hr, rinsed in phosphate buffer overnight, and processed for HRP histochemistry using diaminobenzidine (DAB) as the chromogen. Retinas were incubated in the DAB solution (0.1% in 0.01 M phosphate buffer, pH 7.4) for 5 min. H$_2$O$_2$ (0.03%) was added and the retinas were further incubated for 3–4 min, then rinsed in phosphate buffer overnight. Retinas were whole mounted on slides with polyvinyl alcohol (PVE), coverslipped, and stored refrigerated.

Very large-field cells with thin processes will often be completely but only lightly biotin stained. We have photochemically enhanced lightly stained cells using 0.02% nitro blue tetrazolium (NBT) in 0.1 M Tris buffer (pH 8.2) as described by Vaney (1990). Another method for improving the biotin staining uses biotinylated anti-rhodamine prior to HRP processing. This has the advantage of giving darkly stained cells without the lengthy washing required to remove unreacted NBT from the tissue. Following fixation, retinas were incubated in 0.1% Triton X-100 in PBS (0.1 M, pH 7.4) containing biotinylated anti-rhodamine (C# BA-0605, Vector Labs) at a concentration of 1:100 for $\sim$36 hr at room temperature, then washed in phosphate buffer overnight. Retinas were then processed for HRP histochemistry as described above using the Vector avidin-biotin-HRP complex and DAB.

Brain sections (50 μm thick) were reacted to reveal biotin labeling using the same HRP histochemistry as described above with the following exception. Free floating sections were incubated in the 0.1% Triton X-100/avidin-biotin-HRP solution for 2.5 hr, then washed in phosphate buffer for 2 hr, changing the buffer every 20 min. DAB reaction and slide mounting were the same as described above.

References

Ackroyd, R., Kelty, C., Brown, N., and Reed, M. (2001). The history of photodetection and photodynamic therapy. Photochem. Photobiol. *74*, 656–669.

Born, R.T. (2001). Visual processing: parallel-er and parallel-er. Curr. Biol. *11*, R566–R568.

Briggs, F., and Callaway, E.M. (2001). Layer-specific input to distinct cell types in layer 6 of monkey primary visual cortex. J. Neurosci. *21*, 3600–3608.

Chattipakorn, S.C., and McMahon, L.L. (2002). Pharmacological characterization of glycine-gated chloride currents recorded in rat hippocampal slices. J. Neurophysiol. *87*, 1515–1525.

Dacey, D.M. (2000). Parallel pathways for spectral coding in primate retina. Annu. Rev. Neurosci. *23*, 743–775.

Dacey, D.M., and Lee, B.B. (1994). The blue-ON opponent pathway in primate retina originates from a distinct bistratified ganglion cell type. Nature *367*, 731–735.

Dacey, D.M., and Petersen, M.R. (1992). Dendritic field size and morphology of midget and parasol ganglion cells of the human retina. Proc. Natl. Acad. Sci. USA *89*, 9666–9670.

Dacey, D.M., Lee, B.B., Stafford, D.K., Pokorny, J., and Smith, V.C. (1996). Horizontal cells of the primate retina: cone specificity without spectral opponency. Science *271*, 656–659.

Dacey, D.M., Packer, O.S., Diller, L., Brainard, D., Peterson, B.B., and Lee, B.B. (2000). Center surround receptive field structure of cone bipolar cells in primate retina. Vision Res. *40*, 1801–1811.

Dacey, D.M., Peterson, B.B., and Robinson, F.R. (2002). Identification of an S-cone opponent OFF pathway in the macaque monkey retina: morphology, physiology and possible circuitry. IOVS 43., in press.

DeMonasterio, F.M., and Gouras, P. (1975). Functional properties of ganglion cells of the rhesus monkey retina. J. Physiol. *251*, 167–195.

Diwu, Z., and Lown, J.W. (1994). Phototherapeutic potential of alternative photosensitizers to porphyrins. Pharmacol. Ther. *63*, 1–35.

Dougherty, T.J., Gomer, C.J., Henderson, B.W., Jori, G., Kessel, D., Korbelik, M., Moan, J., and Peng, Q. (1998). Photodynamic therapy. J. Natl. Cancer Inst. *90*, 889–905.

Enroth-Cugell, C., Robson, J.G., Schweitzer-Tong, D.E., and Watson, A.B. (1983). Spatio-temporal interactions in cat retinal ganglion cells showing linear spatial summation. J. Physiol. *341*, 279–307.

Gamlin, P.D.R., Peterson, B.B., and Dacey, D.M. (2001). Physiology and morphology of retinal ganglion cells projecting to the pretectal olivary nucleus of the rhesus monkey. IOVS Suppl. *42*, S676.

Gandin, E., Lion, Y., and Van De Vorst, A. (1983). Quantum yield of singlet oxygen production by xanthene derivatives. Photochem. Photobiol. *37*, 271–278.

He, S., and Masland, R.H. (1998). ON direction-selective ganglion

cells in the rabbit retina: dendritic morphology and pattern of fasciculation. Vis. Neurosci. *15*, 369–375.

Kaplan, E., Lee, B.B., and Shapley, R.M. (1990). New views of primate retinal function. Prog. Retinal Res. *9*, 273–336.

Lee, B.B. (1999). Receptor inputs to primate ganglion cells. In Color Vision: From Genes to Perception, K.R. Gegenfurtner and L.T. Sharpe, eds. (New York: Cambridge University Press), pp. 203–218.

Lee, B.B., Martin, P.R., and Valberg, A. (1988). The physiological basis of heterochromatic flicker photometry demonstrated in the ganglion cells of the macaque retina. J. Physiol. *404*, 323–347.

Lee, B.B., Pokorny, J., Smith, V.C., Martin, P.R., and Valberg, A. (1990). Luminance and chromatic modulation sensitivity of macaque ganglion cells and human observers. J. Opt. Soc. Am. A *7*, 2223–2236.

Lee, B.B., Pokorny, J., Smith, V.C., and Kremers, J. (1994). Responses to pulses and sinusoids in macaque ganglion cells. Vision Res. *34*, 3081–3096.

MacNeil, M.A., and Masland, R.H. (1998). Extreme diversity among amacrine cells: implications for function. Neuron *20*, 971–982.

Martin, P.R., White, A.J.R., Goodchild, A.K., Wilder, H.D., and Sefton, A.E. (1997). Evidence that blue-on cells are part of the third geniculocortical pathway in primates. Eur. J. Neurosci. *9*, 1536–1541.

Masland, R.H. (2001a). The fundamental plan of the retina. Nat. Neurosci. *4*, 877–886.

Masland, R.H. (2001b). Neuronal diversity in the retina. Curr. Opin. Neurobiol. *11*, 431–436.

Masland, R.H., and Raviola, E. (2000). Confronting complexity: strategies for understanding the microcircuitry of the retina. Annu. Rev. Neurosci. *23*, 249–284.

Miller, J.P., and Selverston, A. (1979). Rapid killing of single neurons by irradiation of intracellularly injected dye. Science *206*, 702–704.

Nirenberg, S., and Cepko, C. (1993). Targeted ablation of diverse cell classes in the nervous system in vivo. J. Neurosci. *13*, 3238–3251.

Nirenberg, S., and Meister, M. (1997). The light response of retinal ganglion cells is truncated by a displaced amacrine circuit. Neuron *18*, 637–650.

Packer, O., Diller, L.C., Verweig, J., Lee, B.B., Pokorny, J., Williams, D.R., Dacey, D.M., and Brainard, D.H. (2001). Characterization and use of a digital light projector for vision research. Vision Res. *41*, 427–439.

Perry, V.H., Oehler, R., and Cowey, A. (1984). Retinal ganglion cells that project to the dorsal lateral geniculate nucleus in the macaque monkey. Neuroscience *12*, 1101–1123.

Picaud, S., Wunderer, H., and Franceschini, N. (1990). Dye-induced photopermeabilization and photodegeneration: a lesion technique useful for neuronal tracing. J. Neurosci. Methods *33*, 101–112.

Picaud, S., Peichl, L., and Franceschini, N. (1993). Dye-induced photolesion in the mammalian retina: glial and neuronal reactions. J. Neurosci. Res. *35*, 629–642.

Pu, M., Berson, D.M., and Pan, T. (1994). Structure and function of retinal ganglion cells innervating the cat's geniculate wing: an in vitro study. J. Neurosci. *14*, 4338–4358.

Reiner, A., Veenman, C.L., Medina, L., Jiao, Y., Del Mar, N., and Honig, M.G. (2000). Pathway tracing using biotinylated dextran amines. J. Neurosci. Methods *103*, 23–37.

Rodieck, R.W. (1998). The First Steps in Seeing (Sunderland, MA: Sinauer Associates, Inc.).

Rodieck, R.W., and Watanabe, M. (1993). Survey of the morphology of macaque retinal ganglion cells that project to the pretectum, superior colliculus, and parvicellular laminae of the lateral geniculate nucleus. J. Comp. Neurol. *338*, 289–303.

Sandell, J.H., and Masland, R.H. (1988). Photoconversion of some fluorescent markers to a diaminobenzidine product. J. Histochem. Cytochem. *36*, 555–559.

Sawatari, A., and Callaway, E.M. (2000). Diversity and cell type specificity of local excitatory connections to neurons in layer 3B of monkey primary visual cortex. Neuron *25*, 459–471.

Spikes, J.D. (1991). Applications of dye-sensitized photoreactions in neurobiology. Photochem. Photobiol. *54*, 1079–1092.

Sterling, P. (1998). Retina. In The Synaptic Organization of the Brain, fourth edition, G.M. Shepherd, ed. (New York: Oxford University Press), pp. 205–253.

Vaney, D.I. (1990). The mosaic of amacrine cells in the mammalian retina. Prog. Retinal Res. *9*, 49–100.

Vercelli, A., Repici, M., Garbossa, D., and Grimaldi, A. (2000). Recent techniques for tracing pathways in the central nervous system of developing and adult mammals. Brain Res. Bull. *51*, 11–28.

Wässle, H., and Boycott, B.B. (1991). Functional architecture of the mammalian retina. Physiol. Rev. *71*, 447–480.

Watanabe, M., and Rodieck, R.W. (1989). Parasol and midget ganglion cells of the primate retina. J. Comp. Neurol. *289*, 434–454.

Wayne, C.E., and Wayne, R.P. (2001). Photochemistry. (Oxford: Oxford University).

Weinstein, J.N., Yoshikami, S., Henkart, P., Blumenthal, R., and Hagins, W.A. (1977). Liposome-cell interaction: transfer and intracellular release of a trapped fluorescent marker. Science *195*, 489–492.

White, A.J., Wilder, H.D., Goodchild, A.K., Sefton, A.J., and Martin, P.R. (1998). Segregation of receptive field properties in the lateral geniculate nucleus of a new-world monkey, the marmoset *Callithrix jacchus*. J. Neurophysiol. *80*, 2063–2076.

Yang, G., and Masland, R.H. (1994). Receptive fields and dendritic structure of directionally selective retinal ganglion cells. J. Neurosci. *14*, 5267–5280.